MicroThrust MEMS electrospray emitters – integrated microfabrication and test results

AAAF-ESA-CNES Space Propulsion 2012
7th ï 10th May 2012, Bordeaux, France

Charles Ryan[1] and John P. W. Stark[2]
Queen Mary University of London, London E1 4NS, United Kingdom

Çaĵlar Ataman[3], Simon Dandavino[4], Subha Chakraborty[5] and Herbert Shea[6]
École Polytechnique Fédérale de Lausanne (EPFL), Neuchatel, 2000, Switzerland

ABSTRACT

With the growth of interest in small satellites (<10kg), there is a particular need to provide a propulsion element for this class of spacecraft. Microfabricated electrospray thrusters offer a solution to this problem. By using ionic liquids as the propellant solely ions can be emitted, resulting in a large specific impulse [1]. The thrust from an individual emitter is though a fraction of a εN. However by using well-established MEMS technologies thousands of capillary emitters can be manufactured within an area of a few cm^2, increasing the thrust to the mN level.

We report on results from the Microthrust FP7 Project [1], where the aims are to manufacture and test a complete breadboard thruster system based upon microfabricated thruster chips, alongside the design of a flight system that could enable a CubeSat to leave earth orbit. Prior to this project we had developed a number of manufacturing processes for specific thruster elements [2, 3]. We report here on a new generation of microfabricated emitters, and their relative performance.

The emitters consist of 70 μm high etched-Silicon capillaries with outer diameters tapering to less than 10 μm. Previous designs included 5 μm silica microspheres within the 18 to 24 μm internal diameter of the emitter to increase the hydraulic impedance [4]. However the filling factor of these microspheres in individual emitters differed; therefore a new generation of emitters having more similar impedance and with 5 - 10 μm internal diameters and hole depths of 100 μm have been manufactured.

Previously the etched-Silicon extractor chip was aligned to the emitter chip using 200 μm ruby spheres [2]. Due to assembly difficulties this has been replaced with a polymer-based wafer bonding interface, allowing for simplified assembly and a wafer-scale fabrication process.

These emitters have been tested in both uni-polar and bi-polar mode, using the ionic liquid 1-ethyl-3-methylimidazolium tetrafluoroborate (EMI-BF_4). The tests herein have been achieved without an acceleration stage. The Time-of-Flight data shows a mixed ion-droplet regime, approaching a Purely Ionic Regime (PIR) at low flow rates.

NOMENCLATURE

EPFL	École Polytechnique Fédérale de Lausanne
EMI-BF_4	1-ethyl-3-methylimidazolium tetrafluoroborate
IL	Ionic Liquid
I_{sp}	Specific Impulse
PIR	Purely Ionic Regime
QMUL	Queen Mary, University of London
ToF	Time of Flight
TRL	Technology Readiness Level

INTRODUCTION

With their small size and low power consumption microfabricated electrospray ion sources offer a promising propulsion technology for small (<100 kg) spacecraft. Electrospray emitters operate by transporting a propellant, typically an ionic liquid, to the tip of an emitter. This fluid transport can occur due to wicking in the case of an externally wetted [5, 6] and porous emitters [7, 8], or by an external pressure source and/or wicking for a capillary-like emitter [3, 9-11].

1. www.microthrust.net

1. Post-doc, School of Engineering and Materials Science, c.n.ryan@qmul.ac.uk
2. Professor, School of Engineering and Materials Science, j.p.w.stark@qmul.ac.uk
3. Post-doc, Microsystems for Space Technologies Laboratory (IMT - LMTS), caglar.ataman@epfl.ch
4. PhD Student, Microsystems for Space Technologies Laboratory (IMT - LMTS), simon.dandavino@epfl.ch
5. PhD Student, Microsystems for Space Technologies Laboratory (IMT - LMTS), subha.chakraborty@epfl.ch
6. Associate Professor, Microsystems for Space Technologies Laboratory (IMT - LMTS), herbert.shea@epfl.ch

By the application of a potential difference between the emitter and an opposing electrode a strong electric field is created. This field forces the liquid into a Taylor cone [12], with charged droplets emitted from the cone-jet tip. If though an ionic liquid (IL) is used as a propellant, it has been found that the electric field is sufficiently intense (due to the ionic liquid high surface tension and conductivity [13]) to result in a spray of both ions and droplets. In some cases a Purely Ionic Regime (PIR) occurs, with no droplets present within the plume [1]. This results in a specific impulse of several thousand seconds.
The MicroThrust Project is using the capillary emitter electrospray technique, with an ionic liquid as the propellant. The emitters are microfabricated using Silicon etching processes, which offer good manufacturing precision at the micron level. In the design of the final system the propellant is not pressure-driven, being fed from the propellant chamber using the capillarity forces. This offers greater simplicity than a pressure fed propellant flow system.

Previous work by our group has tailored the hydraulic impedance of the emitter by inserting microbeads within the 18-26 μm inner diameter capillaries. This reduced the overflow of the ionic liquid, and increased the performance of the emitter towards that of PIR [4]. Current efforts continue this trend of applying a high hydraulic impedance, but rather than filling with microbeads the emitter inner diameter is greatly reduced, with a target of 5ε m [14]. These emitters have been successfully operated, with the spray current as a function of voltage, referred to herein as the IV characteristic, and plume angle characteristics investigated, and the Time of Flight (ToF) measurements completed.
This work is carried out in the framework of the MicroThrust project which aims to develop to Technology Readiness Level (TRL-5) a system based on this technology.

CURRENT AND FUTURE BREADBOARD DESIGN

The new generation thruster consists of an emitter and extractor etched Silicon wafer sandwiching a 50 ε m thick polymer layer. A cross section of this assembly is shown in Figure 1. The capillaries stand off the silicon surface by 70 ε m. Each capillary has an individual extractor electrode with a suitably sized orifice. The intention of this layout, with each emitter isolated from the electric field of its neighbour, is to guarantee homogeneous spray characteristics across the array. The extractor electrode chip is electrically isolated from the emitter capillary chip by the polymer layer. The capillary tip is etched to enhance the sharpness of the tip and reduce the total tip area, should the liquid wet the entire top surface.

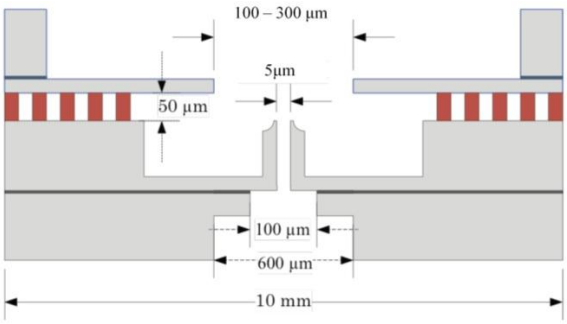

Figure 1: Schematic of current new generation thruster cross-section. Dimensions not to scale. From top to bottom: extractor wafer, insulating bonding layer (red), emitter wafer with etched micron-sized capillary.

Note though that this new emitter design is not the current breadboard thruster design towards which the MicroThrust Project is working, with the most significant omission being the acceleration stage. The breadboard thruster design is illustrated in Figure 2. The extractor and the accelerator electrodes are fabricated on a common glass wafer with electrode layers on each face. This joint electrode stack can be integrated with the capillary wafer using a conventional bonding process.

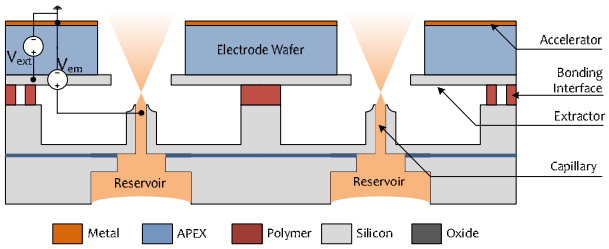

Figure 2: Schematic of breadboard thruster design cross-section.

FABRICATION OF CURRENT EMITTERS

Microfabrication methods offer the batch manufacturing of precision structures with features in the micrometer range. Within the context of an electrospray thruster, the most important advantage of using microfabricated emitters is the possibility of high number of emitters packed within a small area, boosting the thrust density, which is a fundamental limitation for such thrusters. In this work, the two basics components of an electrospray thruster, namely the capillary emitter and the extractor electrode, are fabricated on separate wafers and then integrated through a wafer bonding process. Therefore the major task of assembly with good capillary-extractor alignment (within a few microns) is accomplished.

Emitter & extractor fabrication

The fabrication of the emitters and the extractors are based on silicon-on-insulator (SOI) wafers from a commercial supplier. These wafers consist of a thin silicon oxide (SiO_2) layer sandwiched between two thicker single-crystal silicon layers. This buried oxide acts as a stopping layer during silicon etching, enabling very good height

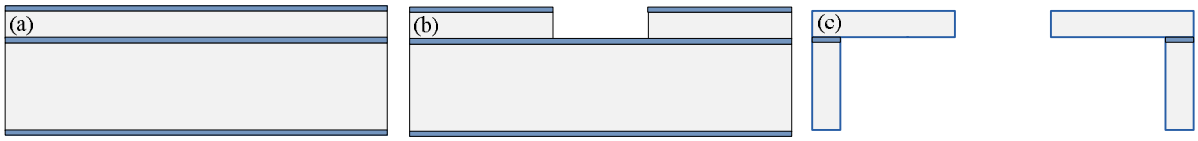

Figure 3. Fabrication steps for the extractor wafers. The SOI wafers have 50 µm thick device layer, 2 µm thick buried.

control for the structures machined on both sides of the wafer. For both the capillaries and the emitters, the process begins with thermal oxidation (2.2 ε m).

In the case of the extractor fabrication, the first lithography, wet oxide etch and the consecutive Deep Reactive Ion Etch (DRIE) define the extractors on the device layer of the extractor wafer, which has 50/2/400 ε m thick device/oxide/handle layers (Figure 3b). The extractor diameter varies from 100 to 300 ε m. A similar set of steps follow for the opening of the extractors from the backside. The thick handle layer acts both as a support layer for the relatively thin extractors and also as a spacer with well-defined thickness between the extractors and a possible integrated accelerator electrode. Finally, the buried oxide and the remaining oxide layers on both faces are removed and the wafers are coated with 200 nm of aluminum on both sides to maintain uniform potential distribution all along the extractor chip (Figure 3c).

The capillary fabrication process involves several more etching and lithography steps. Via the first lithography/wet oxide etch/DRIE sequence the 100 ε m deep capillaries are defined on the device layer. This etch constitutes the most critical step within the process flow due to the very high aspect ratio holes required (Figure 4b). The optimization of the etch parameters is of utmost importance to ensure small capillaries with high hydraulic impedance. The current capillary design has an inner diameter of 5 ε m. For the lithography defining the outer capillary walls, DuPont MX5015 laminated dry photoresist is used since it provides good coverage over the structured surface (Figure 4 c). The emitters are then shaped by an isotropic silicon etch (to increase tip sharpness) and a consecutive DRIE step to create the height of the capillary (Figure 4 d). The capillary fabrication is completed by the definition of a backside reservoir via a two layer etch (Figure 4 f). A stacked photoresist and oxide mask is used for this last backside etch, which is followed by the release of the chips in a wet oxide etching bath.

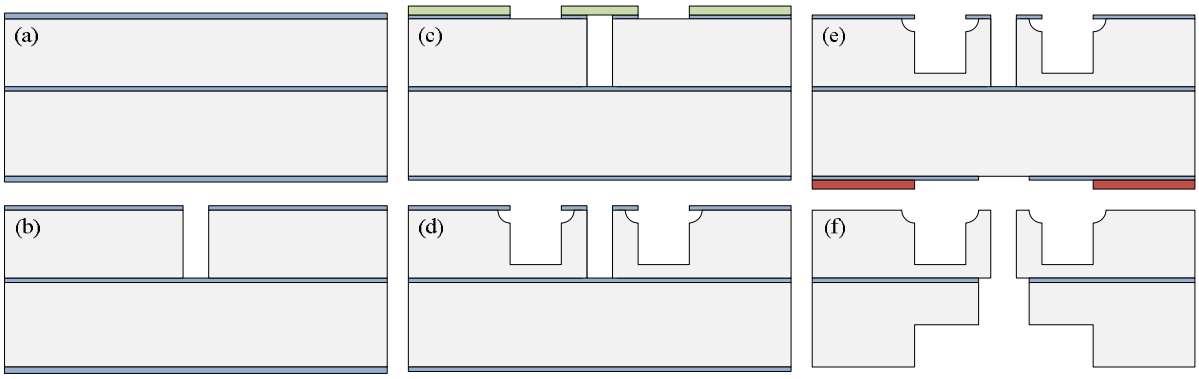

Figure 4: Fabrication steps for the emitter wafers. The SOI wafers have 100 µm thick device layer, 2 µm thick buried oxide layer, and 500 µm thick handle layer. The thermal oxide on both faces is 2.2 µm thick.

Wafer level bonding

For the integration of the capillary and extractor wafers described in the previous subsection, the bonding interface should be electrically isolating with enough dielectric strength to withstand high potential differences between the surfaces, be able to be applied with different thicknesses for design flexibility and optimization, and if possible detachable to enable inspection of the surfaces post-testing. To meet the above requirements, a new bonding method using DuPont MX5000 series laminated dry photoresists was developed. This SU8 based resist film developed for thick electroplating processes is offered in various thicknesses, and has a dielectric strength of 120 kV/mm. A film of 50 ε m thickness can therefore withstand a potential difference of 6 kV, which is significantly larger than the voltages involved in the operation of our devices.

Fundamental steps of the bonding and dicing process are illustrated in Figure 5.

The extractor wafer was chosen as the carrier surface for the bonding polymer. The dry photo resist film is laminated using a semi-automatic lamination tool with roll temperature of 85°C, roll pressure of 2 bars, and roll speed of 1.2 m/min. Post-lamination bake, which enhances the resist adhesion, is avoided. Patterning of the resist is the same as conventional photoresists with an exposure intensity of 110 mJ/cm^2. Alignment of the two wafers prior to the bonding is of utmost importance. A Karl Süss BA6 type bond alignment tool is used for alignment and pre-bonding (5 min @ 125°C with no applied pressure). The actual bonding follows the alignment and is performed with a manual bonding tool under 115 °C and 92 N/cm^2 pressure. After 1 hour, the temperature is gradually decreased down to 50 °C over 45 minutes. After bonding, the stack is sandwiched between two dicing tapes to prevent sample contamination during the mechanical dicing step, by which the wafers are diced into 1 cm by 1 cm thruster chips.

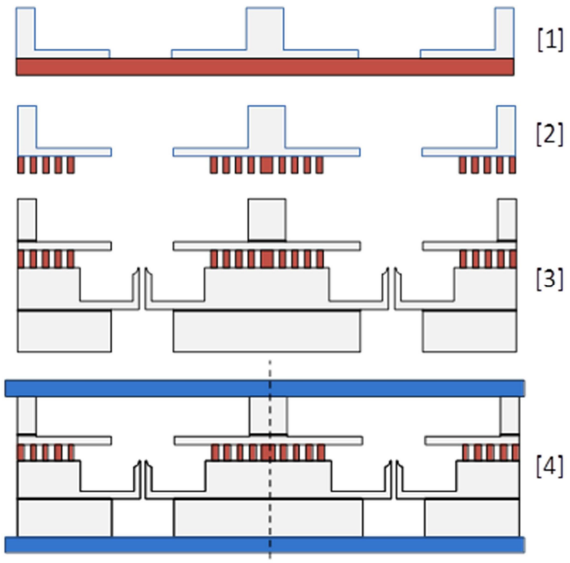

Figure 5: Wafer level assembly process.

The non-permanent (the bonding resist can chemically be removed even after the curing process) wafer level assembly of the emitters and extractor allows the disassembly of the thruster for failure analysis and can provide better than 5 εm alignment. An SEM image of an integrated thruster array is shown in Figure 6.

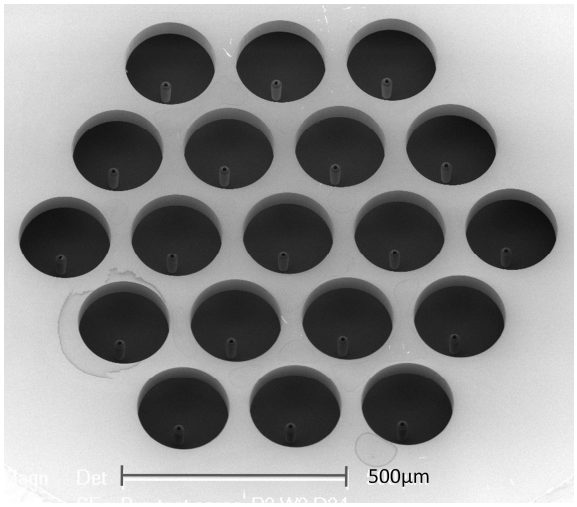

Figure 6: SEM image of an integrated thruster array. The emitter inner diameters are 5 µm, and the extractor diameters are 200 µm.

EXPERIMENTS

The characterization of the thruster test modules reported herein is that of time-of-flight in order to determine the nature of the plume species. A layout of the setup is given in Figure 7. The test bench consists of a 400mm diameter by 400mm long cylindrical vacuum chamber for emitter performance characterization. A second smaller chamber is used as a propellant reservoir, connected to the main chamber by fused silica tubing. The storage of ionic liquid in the absence of background water vapor and other contaminants enables the degassing of the ionic liquid before filling the test module. The base pressure attained in the main chamber is ~ 1×10^{-6} mbar and in the fluid reservoir ~1.3×10^{T3} mbar. For this stage of spray testing the emitter capillaries are connected to a commercial power supply, a FuG PC-controlled high voltage source, whilst the extractor electrodes are grounded. The electrospray currents on the emitter and extractor are measured by two potential divider systems, measuring the voltage drops across two 100kq high power resistors. These two voltmeters are connected to the PC via optically isolated cables, allowing for data logging of current on the emitter and extractor.

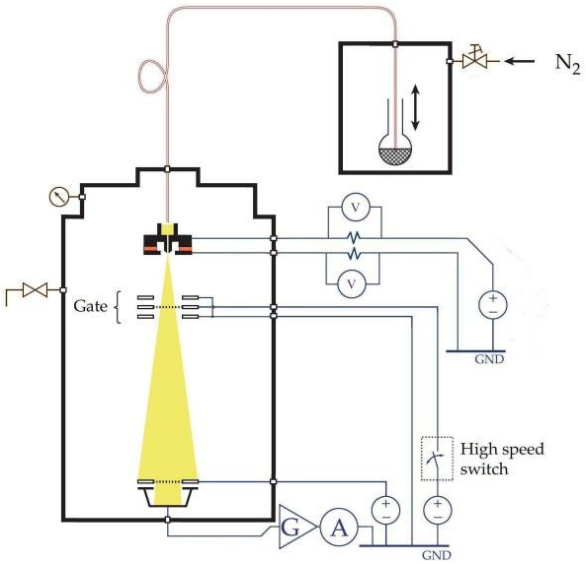

Figure 7: QMUL Time-of-Flight vacuum chamber system for current emitter testing.

A simple electrostatic gate is situated downstream from the emitter, with the gate attached to a DEI PVX-4150 high speed switch, enabling the gate to switch from ground to emitter voltage in ~20 nanoseconds.

The plume is collected on a 70mm diameter flat plate situated up to 400mm downstream, with the option to increase this distance by the addition of a secondary chamber onto the main vacuum chamber. A fine mesh is situated above the plate, to which is applied a negative potential difference to suppress secondary electron emission. The current collected is amplified by a Femto variable-gain high-speed current amplifier. The signal is then supplied to a Wavesurfer oscilloscope for analysis and collection.

Not illustrated in Figure 7is a bipolar relay switch capable of switching between +4kV to -4kV at a frequency of up to 10Hz. This relay can be attached to the emitter connection, allowing for the bipolar spraying, an addition that has been found necessary to avoid electrochemical degradation occurring on the emitter conductive surface [15].

Emitter-extractor chip holder assembly

The current test assembly, partially representative of the eventual thruster module, is a 10mm square emitter-extractor Si chip held within an assembly, as illustrated in

Figure 8. The assembly consists of a central annular aluminum section inserted into an outer PEEK ring. The PEEK ring has a square indentation into which the test chip sits. A EPDM rubber O-ring is positioned in an annular hollow in the Aluminum section, and the chip is fastened down by four bolts. The bolts provide the ground connection to the extractor, whilst the high voltage connection is applied to the central Aluminum section. The ionic liquid propellant can then be fed into the hole through the Aluminum part to the backside of the emitter. We note that this test assembly does not include an accelerator grid, with future testing and the thruster breadboard model including such an electrode.

The propellant is supplied through the fused silica capillary connected onto the test assembly using a nanoport connector (reservoir-fed method), or alternatively by simply allowing drops of propellant to fall from the end of the capillary into the test assembly (gravity-fed method). The respective operational differences of the two different propellant feed systems are described in the penultimate section.

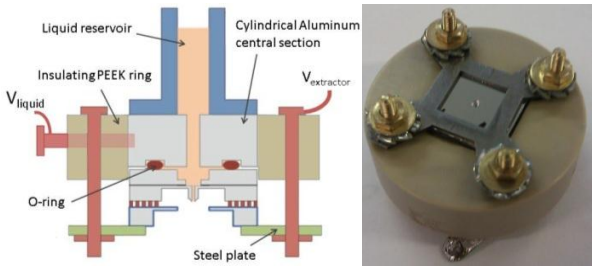

Figure 8: The emitter test assembly, schematic and photo.

Results

ToF data was collected for 5μm emitters in unipolar and bipolar mode using the propellant EMI-BF_4. For the case with the reservoir directly attached to the emitter assembly (reservoir method) a back pressure was applied by pumping N_2 into the reservoir vacuum chamber. The ionic liquid flowed into the emitter assembly where a voltage applied to the emitter resulted in a spray occurring. Figure 9 shows some ToF traces where the reservoir pressure is varied, with the voltage applied being +752V.

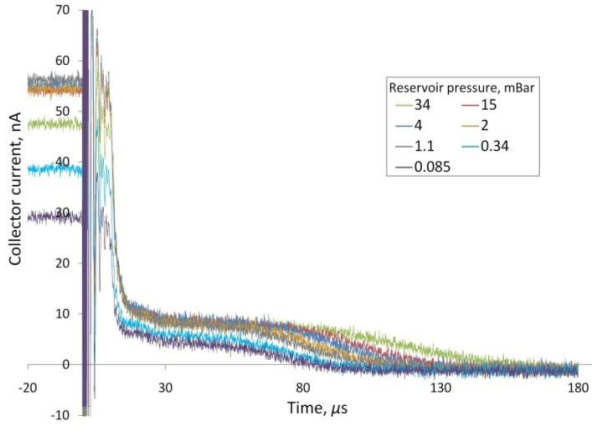

Figure 9: The variation of ToF curves with applied back pressure. Using EMI-BF_4, in uni-polar mode and with a 5μm emitter.

As the back pressure was decreased, the slow droplet tail (i.e. those species detected at longer time intervals) on the TOF traces decreased in length of time, showing that the droplet charge to mass ratio increased, but is not excluded altogether.

From the ToF traces the equivalent specific impulse can be estimated from the current integral under the ToF trace using;

$$I_{sp} = \frac{L_{TOF}}{2\,g_0} \frac{\int_0^\infty i(t)\mathrm{d}t}{\int_0^\infty i(t)\,t\,\mathrm{d}t} \qquad (1)$$

where g_0 is earthôs gravitational constant, L_{TOF} the distance between the ToF gate and the collector plate. The thrust can also be calculated from the ToF trace;

$$T = \frac{2V}{L}\int_0^\infty I(t)dt \qquad (2)$$

Where V is the voltage accelerating the charged particles (assumed to be the applied emitter voltage).
The equivalent I_{sp} values for the ToF traces shown in Figure 9 are illustrated in Figure 10, together with results that were obtained at different emitter voltages. We note that if the test assembly was operating in PIR with solely monomer cations emitted, for an emitter voltage of +752V with no acceleration stage the specific impulse has a theoretical value of 3680s.

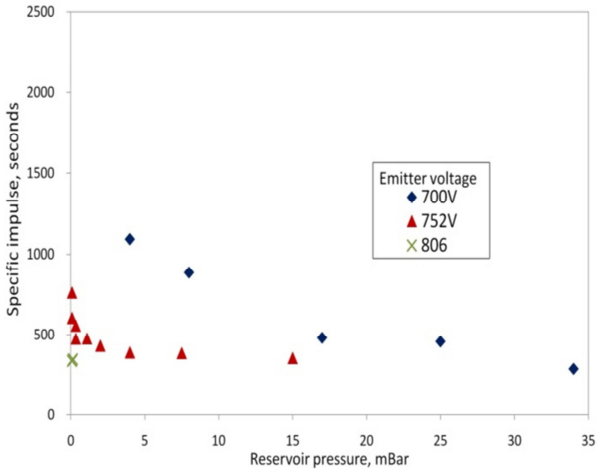

Figure 10: Variation of I_{sp} with reservoir back pressure.

At 752V, as would be expected from the TOF curves in Figure 9, the specific impulse increases as the back pressure is reduced, since the charge to mass ratio of the droplets increases. The same is true for 700V where the specific impulse (with no acceleration) approaches 1100s.

The voltage applied clearly has a significant effect on the performance. At higher emitter voltages reducing the reservoir back pressure had less effect on the specific impulse. Compared to 700V, at 800V the reservoir pressure had to be lower to achieve a certain specific impulse. This observation may be an artifact of the fact that as the voltage is increased, the flow rate from an electrospray emitter has been found to increase (an effect

that may be large for such a small emitter) [16]. With this greater flow rate, the droplets are more inclined to have a higher charge to mass ratio, resulting in a lower specific impulse.

Operating using the reservoir-fed method has though proved to be somewhat difficult because of the ease at which propellant over pressurization can occur. To initiate the spray a large reservoir pressure (generally 100ôs mBar) needs to be applied, and this can result in an oversupply of propellant to the emitter and flooding of the emitter-to-extractor distance. This issue is described in further in the next section.

As an alternative method of propellant feed a gravity-fed method has proven to be more effective. As described above this involves the capillary propellant feed from the reservoir not being directly attached to the emitter assembly, but rather being directly above the assembly rear. Droplets fall from the end of the capillary into a small reservoir within the emitter assembly. This reduces the need to apply a large back pressure, as the constant and controllable pressure head from this small reservoir naturally feeds the emitter with propellant.

Figure 11 illustrates the IV characteristics for positive unipolar spraying, using this method. Ten voltage sweeps are shown. The associated extractor currents are not shown, but were recorded are less than 10nAôs throughout the ten voltage sweeps.

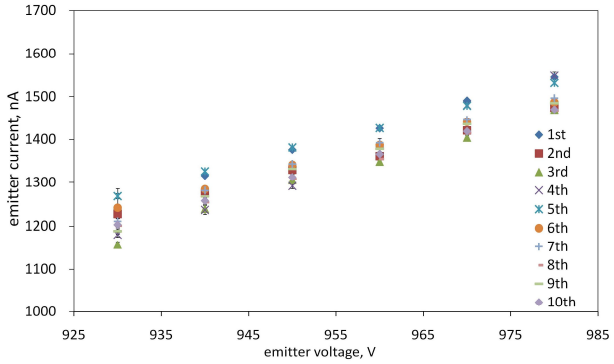

Figure 11: IV plot for unipolar gravity-fed method with positive voltage applied. Ten voltage sweeps were completed.

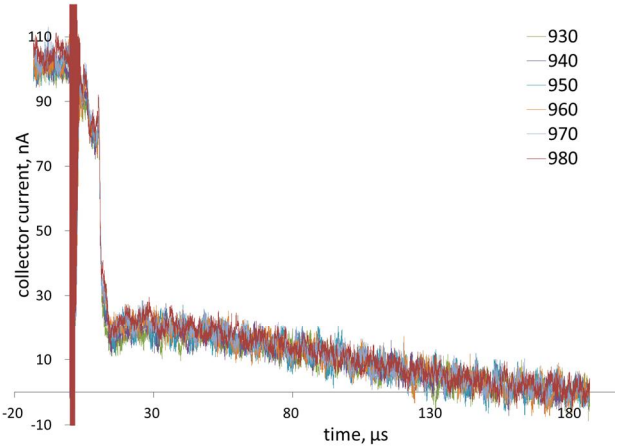

Figure 12: Some representative ToF traces for IV data shown in Figure 11.

Figure 12 illustrates the time-of-flight traces for one of the voltage sweeps shown in Figure 11. These again show a mixture of ions and droplets.

Figure 13 shows the calculated effective I_{sp} and predicted thrust from equations 1 and 2 for a positive unipolar droplet-fed test. The specific impulse is of the order of several hundred seconds, as would be expected for a mixed mode, whilst the thrust is ~0 .2 ï 0.3 εN. Similar performance was found across various experiments.

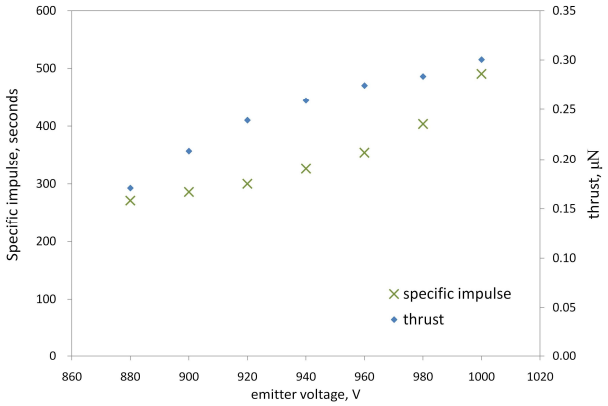

Figure 13: Thrust, I_{sp} data with emitter voltage for gravity-fed method.

Since the MicroThrust Project has the overall aim to produce a breadboard thruster which has the performance to make a mission to near planets or other Near Earth Objects feasible using a small spacecraft, the achieved specific impulse should be of the order of several thousand seconds [17]. Although the breadboard and flight models of the MicroThrust thruster will also include an acceleration grid to increase the specific impulse, on the basis of the results shown in Figure 12 and given the 4kV high voltage power system module that is also being built as part of the MicroThrust project, this acceleration electrode will not improve the performance sufficiently to produce the high I_{sp} required.

To improve the specific impulse sufficiently requires significant suppression, and most probably complete removal of the droplet component of the spray. This can be achieved by reducing the flow rate by further increasing the hydraulic impedance; indeed our group has demonstrated the Purely Ionic Regime using a 19 emitter array filled with microbeads [4]. These results are shown in Figure 14, where a 19 emitter array with 24 μm inner diameter emitter filled with 5 μm microbeads demonstrates PIR.

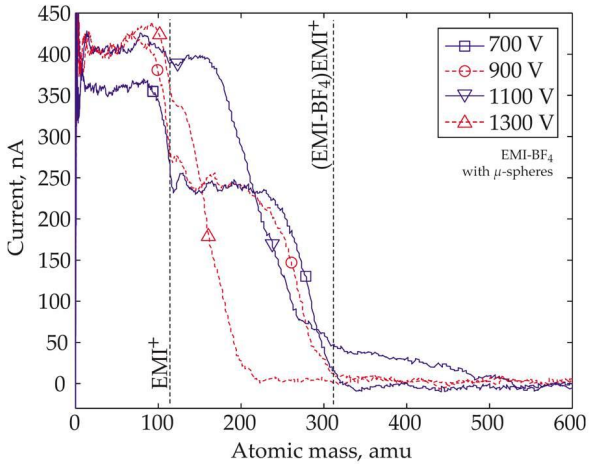

Figure 14: TOF traces recorded with a 19 emitter array with capillaries having a 24 µm inner diameter filled with 5 µm microspheres with an extractor electrode with 200 µm holes space at 90 µm from the capillary tip [4]. Plotted as a function of atomic mass assuming the beam voltage to be equal to the emitter voltage. The masses for the EMI^+ monomer and the $(EMI\text{-}BF_4)EMI^+$ dimer are marked as dotted lines.

Part of the issue with obtaining an ionic regime may be that it has been difficult to create a high enough hydraulic impedance by etching a small diameter capillary, rather than inserting Silica microbeads within a 20 ε m i.d. capillary. This difficulty is illustrated Figure 15, where the hydraulic impedance is plotted against the inner diameter of the emitter. Two vertical lines are shown, one for the current inner diameter of the latest emitter, which because of difficulties in etching holes of small diameter and long depth are on average 9.3 μm rather than the designed 5 μm. The other line shows an empirical estimate of the effective inner diameter of a 20 μm inner diameter emitter filled with 5 μm microbeads. The method is the same as that used by the Yale group to the same situation [11], which by applying the Ergun equation [18] the hydraulic impedance R_T can be calculated;

$$R_T = \frac{\Delta p}{Q} = 150\frac{lv\mu}{D_{bead}^2}\frac{(1-\varepsilon)^2}{Q\varepsilon^3} + 1.75\frac{lv^2\rho}{D_{bead}}\frac{(1-\varepsilon)}{Q\varepsilon^3}. \quad (3)$$

Where Δp is the pressure drop through the bead filled emitter, Q the flow rate, l length of emitter, v velocity of fluid through the emitter, D_{bead} diameter of the bead, μ dynamic viscosity, and ρ the fluid density. ε is the void fraction, which depends upon the packing of the microbeads within the capillary. Here it is taken to be 0.46, in agreement with Lenguito *et al.* [11].

The 2nd part of the RHS of Eq. (3) is small relative to the 1st part; therefore equation (3) can be simplified to;

$$R_T = 600\frac{l\mu}{D_{bead}^2}\frac{(1-\varepsilon)^2}{\pi D_{id}^2\varepsilon^3}. \quad (4)$$

Where D_{id} is the inner diameter of the capillary. This calculated hydraulic impedance can be compared to the effective inner diameter that would result in the same impedance,

$$D_{id,effective} = \sqrt[4]{\frac{\pi R_T}{128\mu l}}. \quad (5)$$

This effective inner diameter and hydraulic impedance of a microbead filled emitter is plotted in Figure 15. This estimate of the hydraulic impedance of the bead-filled emitters is approximately an order of magnitude larger than the impedance of the current emitters. Therefore a larger flow rate for a given applied pressure diference will occur using the non bead-filled emitters, and this may result in a mixed rather than a purely ionic regime.

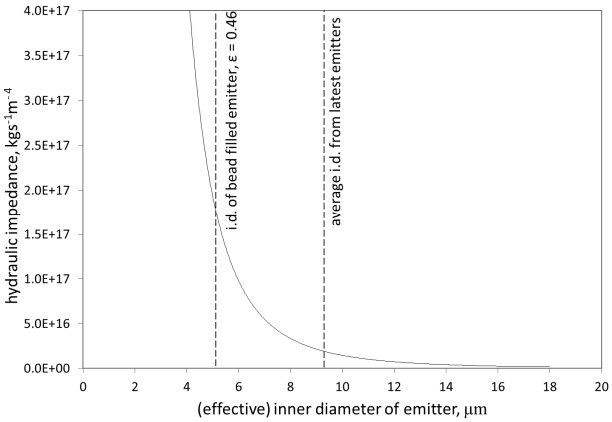

Figure 15: Variation of hydraulic impedance with inner diameter. Inner diameter calculated from latest emitters, and also from bead filled emitter using two methods.

The difficulty in manufacturing these high aspect ratio holes will be resolved with the next generation of emitters currently in fabrication, where the depth of the inner diameter hole is reduced from 100 to 70 ε m, resulting in easier fabrication of this high aspect ratio feature.

Failure modes

As described by previous recent results produced by our group [14], controlling the fluid over the capillary outer surface can be difficult, and can result in the liquid forming a short circuit between the emitter and extractor. Indeed similar problems have been encountered by other groups, with the insertion of microbeads also used to mitigate this problem [10, 11].

This issue has been partially resolved by the detachment of the fluid reservoir, and the filling of the emitter using solely gravitational pressure. It was found that using the reservoir attached to the emitter assembly by a fused silica capillary and a Nanoport connection, could result in the over pressurization of the fluid. Too large a pressure difference could easily be applied between the reservoir and main chamber, resulting in the liquid flooding the emitter-extractor micro-structure. It has been found though that by spraying vertically, with the ionic liquid forming droplets which fall into the backside of the emitter assembly, that spray initialization and operation is considerably easier. Changing to the droplet fed method has resulted in ~90% of the emitter chips operating, compared to approximately a 1/3 operating successfully when the reservoir was directly connected to the emitter assembly. Finally using the droplet-fed method is more

realistic of the MicroThrust breadboard and also eventual flight model, where the emitters are not filled not by an applied reservoir pressure, but by wetting across micromachined Silicon structures.

CONCLUSIONS

Further testing of emitter assemblies as part of the MicroThrust project has revealed the critical need for high hydraulic impedance in the electrospray process. Currently available emitters have not yet achieved the necessary small diameter, however we shall shortly be testing new emitters that will increase the hydraulic impedance by approximately an order of magnitude, which we believe will enable the breadboard model to achieve a specific impulse in the region of 3000s.

ACKNOWLEDGEMENTS

This work was completed within the MicroThrust project, supported by the FP7 Cooperation Work Programme of the European Union.

REFERENCES

[1] I. Romero-Sanz, R. Bocanegra, J. F. d. l. Mora, and M. Gamero-Castano, *"Source of heavy molecular ions based on Taylor cones of ionic liquids operating in the pure ion evaporation regime",* Journal of Applied Physics **94**, 3599-3605 (2003).

[2] R. Krpoun, "*Micromachined electrospray thrusters for spacecraft propulsion*", PhD Thesis, Ecole Polytechnique Fédérale de Lausanne (2008).

[3] R. Krpoun, and H. R. Shea, *"Integrated out-of-plane nanoelectrospray thruster arrays for spacecraft propulsion",* Journal of Micromechanics and Microengineering **19**, 045019 (2009).

[4] R. Krpoun, K. L. Smith, J. P. W. Stark, and H. R. Shea, *"Tailoring the hydraulic impedance of out-of-plane micromachined electrospray sources with integrated electrodes",* Applied Physics Letters **94**, 163502 (2009).

[5] P. Lozano, B. Glass, and M. Martinez-Sanchez, "*Performance Characteristics of a Linear Ionic Liquid Electrospray Thruster*", in 29th International Electric Propulsion Conference, (Princeton University, 2005), IEPC-2005-2192.

[6] P. Lozano, and M. Martínez-Sánchez, *"Ionic liquid ion sources: characterization of externally wetted emitters",* Journal of Colloid and Interface Science **282**, 415-421 (2005).

[7] R. S. Legge, and P. Lozano, *"Electrospray Propulsion Based on Emitters Microfabricated in Porous Metals",* Journal of Propulsion and Power **27**, 485-495 (2011).

[8] D. G. Courtney, and P. Lozano, "*Development of Ionic Liquid Electrospray Thrusters using Porous Emitter Substrates*", in 27th International Symposium on Space Technology and Science,, (Tsukuba, Japan, 2009), ISTS-2009-b-2051.

[9] R. Krpoun, M. Raber, and H. R. Shea, "*Microfabrication and test of an integrated colloid thruster*", in Mems 2008: 21st Ieee International Conference on MEMS, (New York, 2008), 964-967.

[10] G. Lenguito, J. Fernandez de la Mora, and A. Gomez, "*Design and Testing of Multiplexed Electrospray with Post-Acceleration for Space Propulsion Applications*", in 47th AIAA/ASME/SAE/ASEE Joint Propulsion Conference & Exhibit, (San Diego, California, 2011), AIAA 2011-5590.

[11] G. Lenguito, J. Fernandez de la Mora, and A. Gomez, "*Multiplexed Electrospray for Space Propulsion Applications*", in 46th AIAA/ASME/SAE/ASEE Joint Propulsion Conference & Exhibit, (Nashville, TN, 2010), AIAA 2010-6521.

[12] G. Taylor, *"Disintegration of Water Drops in an Electric Field",* Proceedings of the Royal Society of London. Series A, Mathematical and Physical Sciences **280**, 383-397 (1964).

[13] M. Gamero-Castaño, and J. Fernández de la Mora, *"Direct measurement of ion evaporation kinetics from electrified liquid surfaces",* The Journal of Chemical Physics **113**, 815-832 (2000).

[14] S. Dandavino, C. Ataman, H. Shea, C. Ryan, and J. P. W. Stark, "*Microfabrication of Capillary Electrospray Emitters and ToF Characterization of the Emitted Beam*", in 32nd International Electric Propulsion Conference, (Wiesbaden, Germany, 2011), IEPC-2011-2131.

[15] P. Lozano, and M. Martínez-Sánchez, *"Ionic liquid ion sources: suppression of electrochemical reactions using voltage alternation",* Journal of Colloid and Interface Science **280**, 149-154 (2004).

[16] C. N. Ryan, K. L. Smith, M. S. Alexander, and J. P. W. Stark, *"Effect of emitter geometry on flow rate sensitivity to voltage in cone jet mode electrospray",* Journal of Physics D: Applied Physics **42**, 155504 (2009).

[17] F. Tata Nardini *et al.*, "*Devlopment of the MicroThrust breadboard: a miniaturized electric propulsion system for nanosatellites* ", in AAAF-ESA-CNES Space Propulsion Conference 2012, (Bordeaux, France, 2012).

[18] S. Ergun, *"Flow through packed columns",* Chemical engineering Progress **48**, 89 - 94 (1952).